

TranSplat: Lighting-Consistent Cross-Scene Object Transfer with 3D Gaussian Splatting

Tony Yu^{1*} Yanlin Jin^{1*} Ashok Veeraraghavan¹ Akshat Dave² Guha Balakrishnan¹

¹Rice University ²MIT

{tony.yu, yanlin.jin, vashok, guha}@rice.edu ad74@media.mit.edu

<https://tonyyu0822.github.io/transplat/>

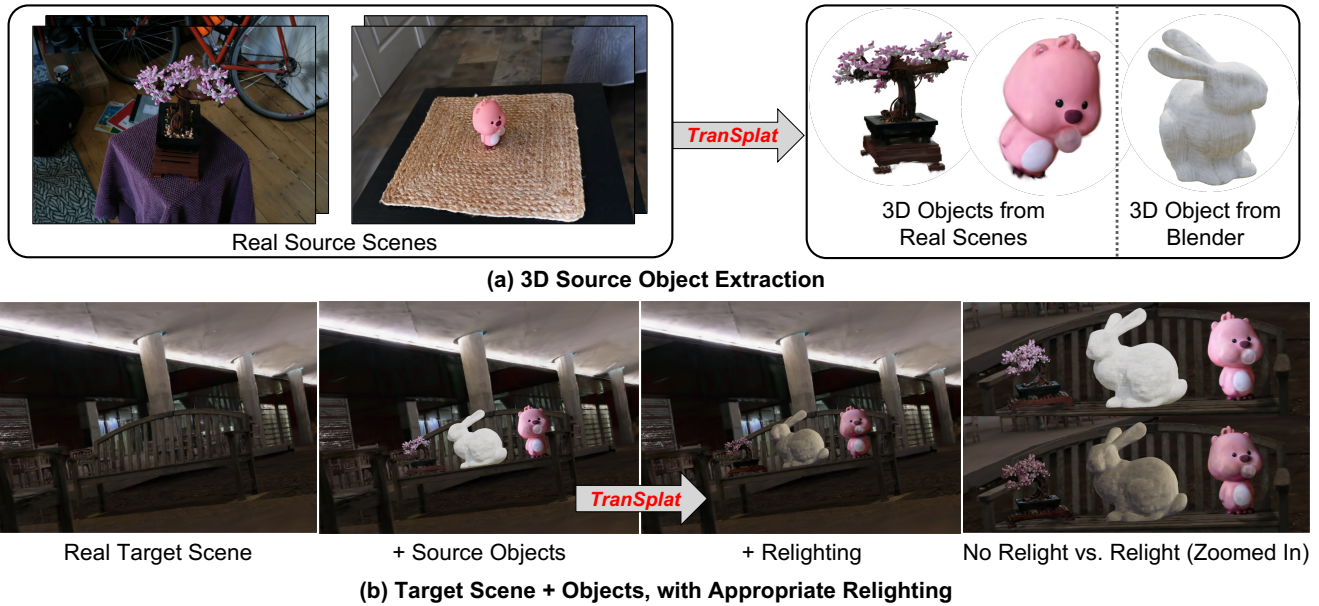


Figure 1. **Example result using *TranSplat* to transfer 3D objects from source scenes to a target scene.** *TranSplat* is an algorithm building on the Gaussian Splatting (GS) [19] framework that (a) extracts 3D objects from GS representation of “source” scenes, and (b) adds them to the GS models of a “target” scene with appropriate appearance modifications consistent with the target lighting conditions.

Abstract

We present *TranSplat*, a 3D scene rendering algorithm that enables realistic cross-scene object transfer (from a source to a target scene) based on the Gaussian Splatting framework. Our approach addresses two critical challenges: (1) precise 3D object extraction from the source scene, and (2) faithful relighting of the transferred object in the target scene without explicit material property estimation. *TranSplat* fits a splatting model to the source scene, using 2D object masks to drive fine-grained 3D segmentation. Following user-guided insertion of the object into the target scene, along with automatic refinement of position and orientation, *TranSplat* derives per-Gaussian radiance transfer

functions via spherical harmonic analysis to adapt the object’s appearance to match the target scene’s lighting environment. This relighting strategy does not require explicitly estimating physical scene properties such as BRDFs. Evaluated on several synthetic and real-world scenes and objects, *TranSplat* yields excellent 3D object extractions and relighting performance compared to recent baseline methods and visually convincing cross-scene object transfers. We conclude by discussing the limitations of the approach.

1. Introduction

The Gaussian Splatting (GS) framework has demonstrated remarkable power and computational speed for differen-

* Equal contribution.

tiable rendering applications [19]. In contrast to Neural Radiance Fields (NeRFs) [28], GS explicitly represents a scene with primitive shapes with optimizable location and appearance parameters. This allows, in particular, the potential to decompose a 3D scene into semantic components. Some recent methods, such as GaussianEditor [9] and DGE [8], leverage this property for interactive 3D scene manipulation, such as changing the color of an existing object or inserting a text-generated object into the scene. In this study, we explore using this property to address a fundamental scene editing task: transferring a 3D object from one scene to another with appropriate relighting effects (see Fig. 1).

This task has two key challenges. First, the object from the “source” scene must be precisely extracted in 3D and placed within the second “target” scene with reasonable orientation/alignment. In addition, the object’s appearance is caused by a combination of material properties and environment lighting effects. Therefore, the second challenge is to apply the appropriate relighting function to the object’s appearance that both removes the source scene’s environment effects, and adds the target scene’s environment effects. Relighting an object under novel illumination conditions is inherently ill-posed due to the intertwined effects of object properties, illumination, and inter-object reflections [4].

We propose *TranSplat* to address these challenges (see Fig. 2). *TranSplat* assumes input image views from a source scene with an object of interest (delineated with a 2D binary mask per image), and input views of a target scene in which to place the object. *TranSplat* first fits a Gaussian Surfels model [10] to the source and 3DGS model to target scenes, and extracts the object from the source model by propagating the 2D object masks to 3D space during fitting. After a user inserts the object into the target scene, *TranSplat* relights the object to be consistent with the target environment by exploiting a theoretical identity relating the spherical harmonic (SH) coefficients of surfaces with radially symmetric BRDFs (e.g., Lambertian or Phong) under different lighting conditions [24]. Building on this identity for GS, *TranSplat* computes radiance transfer functions applied to the SH appearance coefficients of each Gaussian belonging to the transferred object. These functions further rely on a novel approach to sampling environment maps directly from a GS model without additional information. The full relighting pipeline *requires no explicit estimation of surface properties such as BRDFs*.

Our work is closely related to several recent object relighting methods built on the GS framework. These methods all use inverse rendering pipelines that explicitly estimate shading functions, learnable lighting representations, and material properties [14, 16, 22]. Powerful when accurate, these estimations are nevertheless prone to errors on natural scenes due to the ill-posed challenge of disentangling surface reflectance from lighting intensity, leading to

color/tonal shifts, incorrect intensity scaling, and/or noise artifacts in rendering. *TranSplat* offers a complementary approach to these existing methods, bypassing the need to explicitly estimate scene properties, at the cost of ignoring more complex lighting effects such as specularities. In practice, we find that for many scenes, this tradeoff is acceptable, resulting in visually realistic renderings (see Fig. 1).

We evaluated *TranSplat* using a custom synthetic dataset of Lambertian objects generated by a graphics engine, and non-Lambertian objects from the TensoIR dataset [17]. *TranSplat* achieves state-of-the-art qualitative and quantitative performance compared to baseline GS [22] and NeRF [17] relighting methods. We also qualitatively evaluated *TranSplat* on cross-scene transfer with several real indoor and outdoor scenes and objects sourced from the MipNeRF-360 dataset [2], and our own collected scenes. *TranSplat* achieves realistic rendering across all these scenes in terms of object extraction, insertion, and relighting. In summary, the contributions of this study are:

- **Improved fine-grained object extraction in GS** by optimizing per-Gaussian object label weights into the scene fitting process;
- **A new scene relighting strategy in GS** that adapts each Gaussian’s appearance to the target environment by modulating SH coefficients, without requiring explicit object BRDF estimation;
- **A strategy to approximate environment maps** by sampling coefficients directly from a GS model, without any additional supervision;
- **State-of-the-art performance** on relighting and realistic cross-scene appearance adaptation compared to existing GS methods.

2. Related work

Our work falls under the broad umbrella of *inverse rendering*, or the estimation of underlying physical properties of a scene, such as lighting, surface normals, and materials, given images. Classical inverse rendering techniques relied on iterative optimizations using physics, geometry, and signal processing cues [5, 11, 12, 24, 25, 29]. Due to the ill-posedness of the task, classical methods typically focused on controlled setups, and/or apriori known scene properties.

The first inverse rendering methods using deep learning relied on typical feed-forward networks trained over large labeled datasets to predict attributes such as color, shape, and other material properties [21, 31, 36]. Neural radiance fields (NeRFs) [1, 2, 28] spawned a paradigm shift in inverse rendering, relying on a per-scene optimization driven by a multilayer perceptron (MLP) scene encoding and rendering objective. Following methods such as Nerf-in-the-Wild [26] and NeRD [6] demonstrated that “transient” lighting effects may be separated from constant scene properties from image collections. Several NeRF-derived methods ex-

plore deeper integration of physically-based rendering techniques with MLPs to disentangle object-specific and lighting properties [33, 35, 38, 39]. Tensorial Inverse Rendering (TensoIR) further combines MLPs with tensor factorization to yield a representation with lower computational cost and facilitating second-bounce ray marching [17].

Several recent inverse rendering and relighting methods now build on the 3D Gaussian Splatting (GS) [19] framework, and operate using physically-based rendering to estimate surface properties for each Gaussian in a scene [14, 16, 22, 30]. When relying solely on single-environment captures, these methods often struggle to disentangle lighting from material properties. Drawing insight from a theoretical radiance transfer identity in 2D [24] (described in Sec. 3) based on spherical harmonics, we instead propose a complementary approach to radiance transfer in GS that avoids estimating material properties. This strategy sacrifices some of the expressive power of the existing physically-based rendering solutions, but offers a simple, robust solution that is visually appealing (see Fig. 1).

Finally, our work relates to a handful of recent studies that perform GS scene editing tasks [8, 9, 27, 32, 34, 37, 40]. Of these, a closely related work is GaussianEditor [9], which can perform operations such as changing the color of objects and inserting objects generated by text-to-image generative models into GS scenes. *TranSplat* builds on GaussianEditor’s strategy of augmenting each Gaussian in a GS model with additional object labels to perform 3D segmentation. However, unlike GaussianEditor, *TranSplat* optimizes the labels during GS fitting leading to improved performance (see Sec. 4.2).

3. Background: Radiance Transfer Using Spherical Harmonics

We build on a theoretical framework for radiance transfer with spherical harmonics (SHs), originally presented for 2D images only, that obviates the need to estimate bidirectional reflectance distribution functions (BRDFs) assumed to be radially symmetric (e.g., Lambertian or Phong) [24]. We present the concept here.

Consider a point \mathbf{x} on a 3D surface with surface normal $\mathbf{n} = (\alpha, \beta)$, and radially symmetric BRDF $\rho(\theta)$. The rendering equation [18] states:

$$B(\mathbf{n}) = \int_{\Omega} \rho(\theta) L(\omega) (\mathbf{n} \cdot \omega) d\omega, \quad (1)$$

where $B(\mathbf{n})$ is the outgoing radiance at \mathbf{x} , $L(\omega)$ is the incoming radiance from direction $\omega = (\theta, \phi)$, and Ω represents the hemisphere above the point \mathbf{x} . Using spherical harmonic bases $Y_{lm}(\theta, \phi)$, we obtain the following:

$$L(\theta, \phi) = \sum_{l=0}^L \sum_{m=-l}^l L_{lm} Y_{lm}(\theta, \phi), \quad (2)$$

$$B(\alpha, \beta) = \sum_{l=0}^L \sum_{m=-l}^l B_{lm} Y_{lm}(\alpha, \beta), \quad (3)$$

$$\rho(\theta) = \sum_{l=0}^L \rho_l Y_{l0}(\theta). \quad (4)$$

It can be shown that in the frequency domain, each coefficient B_{lm} is given by a simple product formula [3, 29]:

$$B_{lm} = A_l L_{lm}, \quad (5)$$

where $A_l = \sqrt{4\pi/(2l+1)}\rho_l$. Assuming A_l is constant for the object across scenes, we obtain the following relation when imaging the surface in two environments S and T :

$$\frac{B_{lm}^T}{B_{lm}^S} = \frac{L_{lm}^T}{L_{lm}^S} = H_{lm} \implies B_{lm}^T = B_{lm}^S H_{lm}, \quad (6)$$

where H_{lm} is referred to as the *lighting transfer function*. Hence, we may obtain the reflectance of the object in T by multiplying its reflectance in S with the transfer function (on a per-coefficient basis). Crucially, H can be computed purely from the environment lighting maps of S and T , without needing to compute surface material properties.

4. Methods

We assume N_S input images of a source scene S , and N_T images of a target scene T . We also assume N_S binary masks segmenting the object of interest in each of the source images. In our experiments, we use SAM [20] to automatically segment an object from the images given text. We aim to extract the object from S , and render arbitrary views of the object inserted into T with realistic lighting.

To accomplish this, we propose *TranSplat* (see Fig. 2). *TranSplat* first builds separate GS models for S and T . For S , *TranSplat* optimizes an additional, semantic object label per Gaussian that facilitates object extraction. After a human user places the extracted object into T , *TranSplat* performs object relighting building on the concepts introduced in Sec. 3. In particular, we rescale the spherical harmonic (SH) appearance coefficients of the object’s Gaussians based on the ratio of SH coefficients of the estimated environment maps of S and T . We describe *TranSplat*’s components in the following sections.

4.1. GS Model Fitting for S and T

We first fit GS models to both S and T using the input images. For S , we use the Gaussian Surfels model [10]. Unlike the 3D Gaussian ellipsoids used in the original Gaussian Splatting study [19], Gaussian surfels are flattened along one dimension, yielding 2D ellipses with explicit normal directions. As a result, representing a scene with

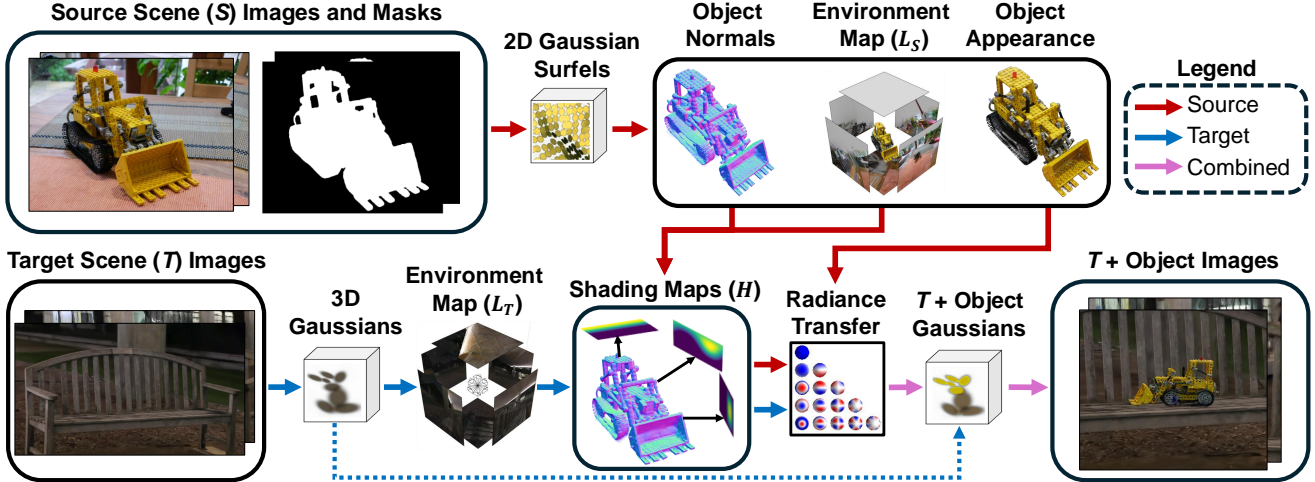


Figure 2. **Overview of TranSplat.** (Top) *TranSplat* fits a Gaussian Surfels [10] model of the source scene (S) from images and object masks. Optimizing per-Gaussian object labels, *TranSplat* extracts the object (and normals) from S , along with an environment map estimated by rendering a cubemap centered around the object based on Gaussian radiance values in the model. (Bottom) *TranSplat* fits a 3D Gaussian Splatting model to the target scene T , and estimates an environment map based on the location and scale of the object (determined by a human user). Using S and T 's environment maps along with the object normals, we relight the object by rescaling the spherical harmonic (SH) appearance coefficients of each of its Gaussians. In particular, we rescale SH coefficients by the ratio of T to S 's environment map SH coefficients, modulated by a shading map measuring the radiance contribution of each environment map pixel to each Gaussian. We use the final merged splatting model to render novel views of the object in T .



Figure 3. **Example of TranSplat extracting fine details of an object when fitting a GS model to a source scene (Sec. 4.2).** *TranSplat* takes input 2D masks, such as the one on the left (generated by SAM [20]), which do not capture fine details such as the flower tendrils. *TranSplat* learns to associate the tendrils with the rest of the vase during optimization due to passing object labels from parent to child Gaussians during densification. The final mask (right) is generated by rasterizing the optimized 3D Gaussian labels into a 2D image.

2D Gaussians yields more accurate estimates of the surface normals of an object, which is crucial for relighting in *TranSplat* (Sec. 4.3). However, we use a standard GS model for T , because we find that 3D Gaussians model unconstrained scenes, such as outdoor environments, better than 2D surfels. As our final renderings are in T , it is imperative that the entire scene (not just an object) is well modeled.

4.2. Object Extraction from S and Insertion into T

To facilitate object extraction from S , we include an additional score variable per 2D Gaussian surfel for S , quantifying the surfel's likelihood of belonging to the object of interest. We update these scores during model fitting by propagating information from the 2D input masks to 3D

space. After fitting this model, we then simply extract all Gaussians with scores greater than a threshold.

Specifically, following GaussianEditor [9], we equip each Gaussian j with a scalar score w_j computed by:

$$w_j = \frac{\sum_{k=1}^{N_S} \sum_{p=1}^P M^k(p) \cdot \tau_j^k(p)}{\sum_{k=1}^{N_S} \sum_{p=1}^P \mathbb{1}(M^k(p))}, \quad (7)$$

where p is a pixel index, $M^k(\cdot)$ is the k -th binary mask (with values of 1 for the object), P is the total number of pixels per image (assuming uniform size), $\mathbb{1}(\cdot)$ is the indicator function, and $\tau_j^k(\cdot)$ is the transmittance function returning a low value for Gaussian j if it has small contribution to rendering pixel p of image k . However, unlike GaussianEditor, we optimize w_j during (instead of after)

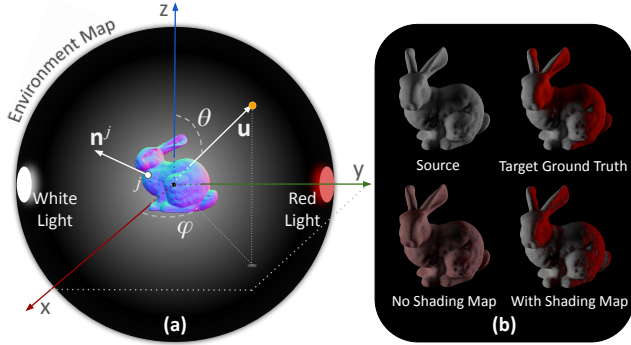


Figure 4. **Conceptual schematic of the shading map computation for a simple scene.** (a) The shading map measures the contribution of each point in an environment map on each Gaussian surfel j of the object (here, a bunny). The contribution is based on the angular alignment of the surfel’s normal \mathbf{n}^j with the point. In this example, Gaussian j would not be strongly affected by the point along \mathbf{u} with orientation (θ, ϕ) . (b) Without applying the shading map, all Gaussians receive input from all environment map points, resulting in a uniform appearance, whereas with shading, accurate colors and shadows are rendered.

model fitting, allowing the scores to propagate from parent to children Gaussians in the “densification” process. We find that this strategy is able to capture fine object details not contoured in the initial 2D masks, as fitting progresses (see Fig. 3).

Once extracted, we expect a user to manually place the object into T via GUI interface [15] with an appropriate position and scaling factor. We further automatically refine the orientation and position of the object using RANSAC [13] so that it flushly sits on the nearest flat surface in T (see Supplementary for details.).

4.3. Cross-Scene Object Relighting

Once the object is placed with correct position, orientation and scale in T , *TranSplat* applies relighting factors to each of the object’s Gaussians so that it has consistent appearance with T ’s environment. To do so, we extend the relation in Eq. 6 to GS. In particular, unlike the 2D case studied by Mahajan et al. [24], each element of the 3D environment maps $L_S(\theta, \phi)$ and $L_T(\theta, \phi)$ will not equally affect the appearance of every Gaussian in a GS model. In fact, for solid objects, we would expect an object’s Gaussians to occlude one another from different portions of the environment lighting. The impact of each point in the environment on a Gaussian must be modulated by the degree to which that Gaussian faces that point (see Fig. 4). To that end, for Gaussian j with normal vector \mathbf{n}^j , we compute a modulated environment map:

$$L_S^j(\theta, \phi) = L_S(\theta, \phi) \cdot H^j(\theta, \phi), \quad (8)$$

where $\mathbf{u}_{\theta, \phi}$ is the unit vector oriented at (θ, ϕ) , and $H^j(\theta, \phi) = \max\{\mathbf{n}^j \cdot \mathbf{u}_{\theta, \phi}, 0\}$ is a *shading map*. We perform the analogous computation to produce $L_T^j(\theta, \phi)$, and arrive at the lighting transfer function for Gaussian j (in SH coefficients):

$$\tau_{lm}^j = L_{T,lm}^j / (L_{S,lm}^j + \varepsilon), \quad (9)$$

where ε is a small constant. In practice, we limit the maximum value of τ_{lm}^j to 1 for stability.

4.3.1. Estimating Environment Maps

Global environment maps $L_S(\theta, \phi)$ and $L_T(\theta, \phi)$ are needed in Eq. 8. Assuming these are unknown, we propose a strategy to estimate environment maps directly from a trained GS model, and approximate their SH coefficients.

We first render the incoming radiance from six orthogonal viewing angles centered around the object in a given scene, forming the six faces of a cubemap. We then create an equirectangular environment map by linking each spherical coordinate of this map to a cubemap face, and sampling the corresponding pixel value. We use an end-to-end LDR-to-HDR model [23] to convert the environment map into HDR format. Finally, to account for a possible rotation of the inserted object, we apply a corresponding rotation to S ’s environment map.

Next, we estimate SH coefficients for each environment map by sampling their values and performing a least squares fit. We empirically find that a uniform sampling strategy over-represents certain regions of the environment map, leading to tonal inaccuracies during rendering. In particular, consider the differential term $d\omega$ from Eq. 1. In a spherical representation, $d\omega = \sin(\theta) d\theta d\phi$, meaning that light contributions from $\theta \approx 0$ and $\theta \approx \pi$ are far smaller than the contribution from $\theta \approx \pi/2$. To compensate for this disparity, we sample values from an environment map proportional to their $\sin(\theta)$ factors.

5. Experiments

We present results using image data from the *MipN-eRF360* [2] and *TensorIR-Synthetic* [17] datasets, swapping objects between scenes with significantly different lighting conditions. We evaluate object extraction in Sec. 5.1, relighting in Sec. 5.2, and cross-scene transfer in Sec. 5.3. We conducted all of our training and rendering processes on an NVIDIA A100 (40 GB) or GeForce RTX 3090 Ti GPU.

5.1. Qualitative Object Extraction Results

We first qualitatively demonstrate *TranSplat*’s ability to perform 3D semantic segmentation of an object, compared to recent Gaussian Splatting segmentation methods: GaussianEditor [9] and SAGA [7]. We experiment with two versions of GaussianEditor: (1) the public model that does not

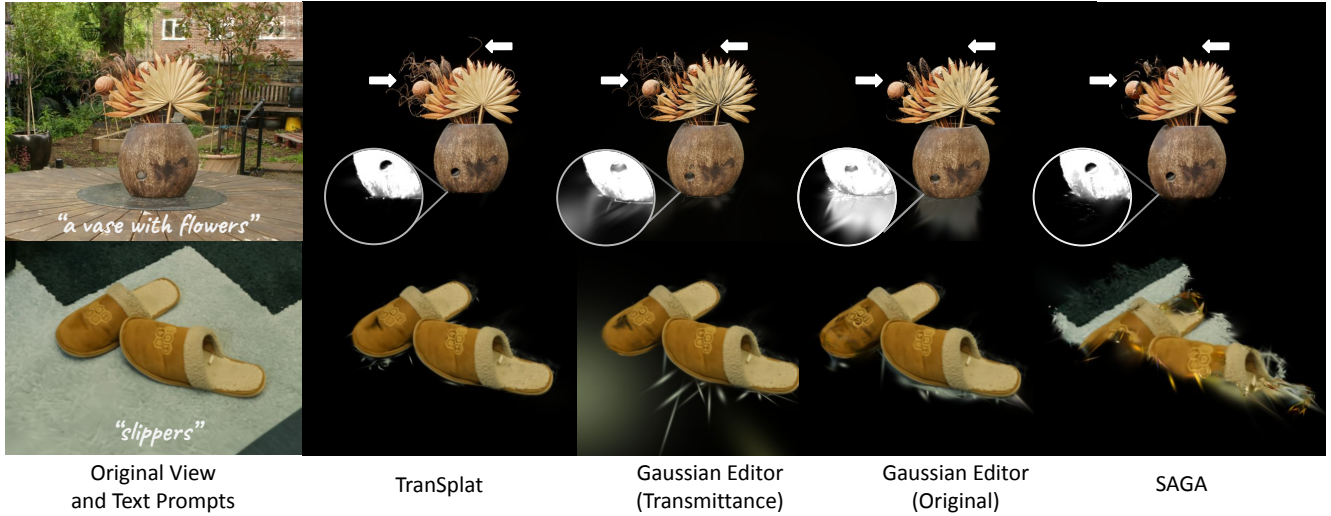


Figure 5. **Sample object segmentation results using *TranSplat* and other 3D rendering baselines.** We compare *TranSplat* against GaussianEditor [9] and SAGA [7]. For the vase, *TranSplat* is best at both recovering the tendrils (indicated with white arrows), which are particularly challenging because they are thin and wiry structures, and delineating the boundary between the bottom of the vase and the table. For the slippers, both GaussianEditor and SAGA leave many spurious background Gaussians associated with the foreground.

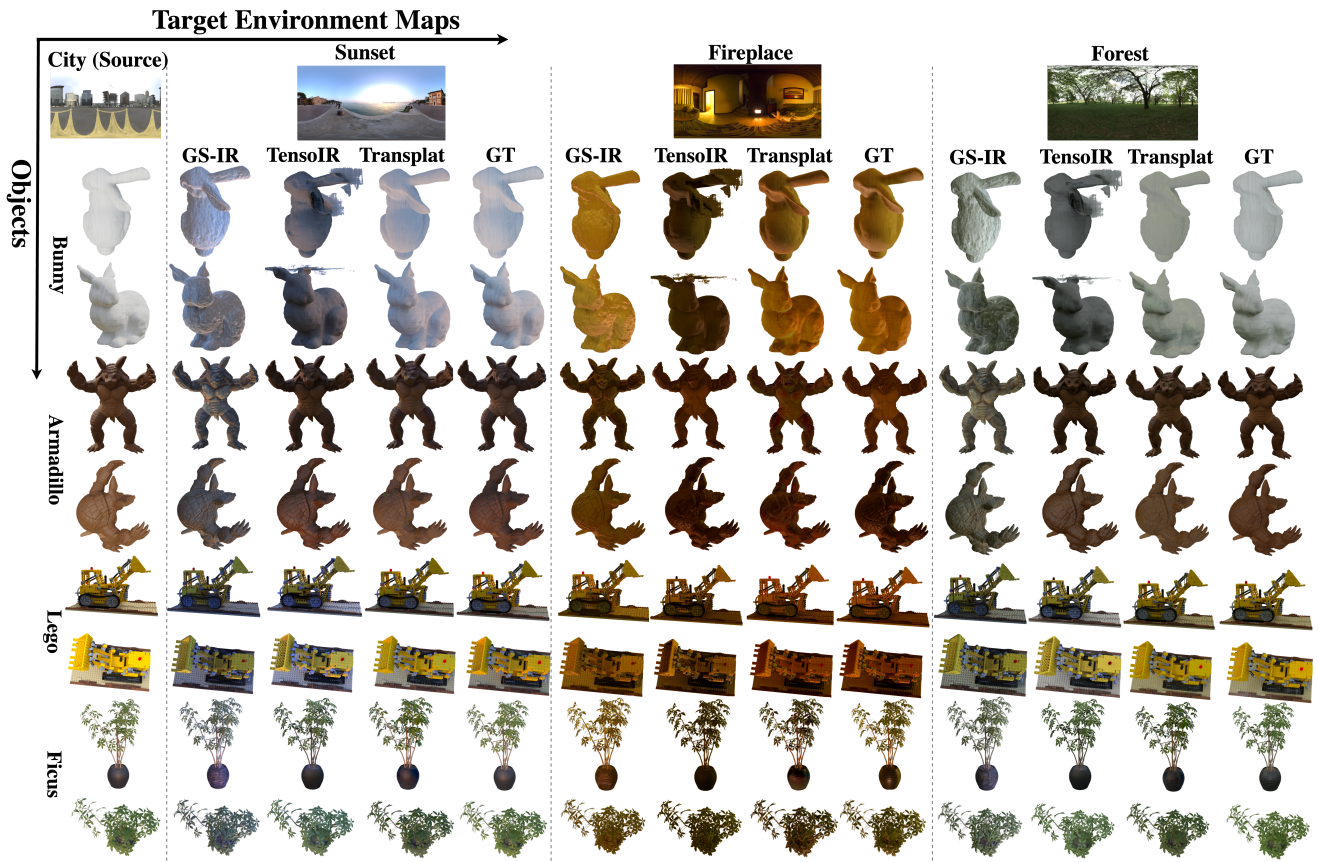


Figure 6. **Relighting results using one Blender-generated (Bunny) and three TensoIR [17] objects.** We apply the same (HDR) source environment map (*City*) to all three objects, and then relight them to three other environment maps: *Sunset*, *Fireplace*, and *Forest*. *TranSplat* achieves almost identical color and shading effects to ground truth (GT). Tenso-IR [17] is comparable in performance on Armadillo, Lego and Ficus, but has significant artifacts on Bunny. GS-IR [22] produces consistently worse results. See Table 1 for corresponding metrics.

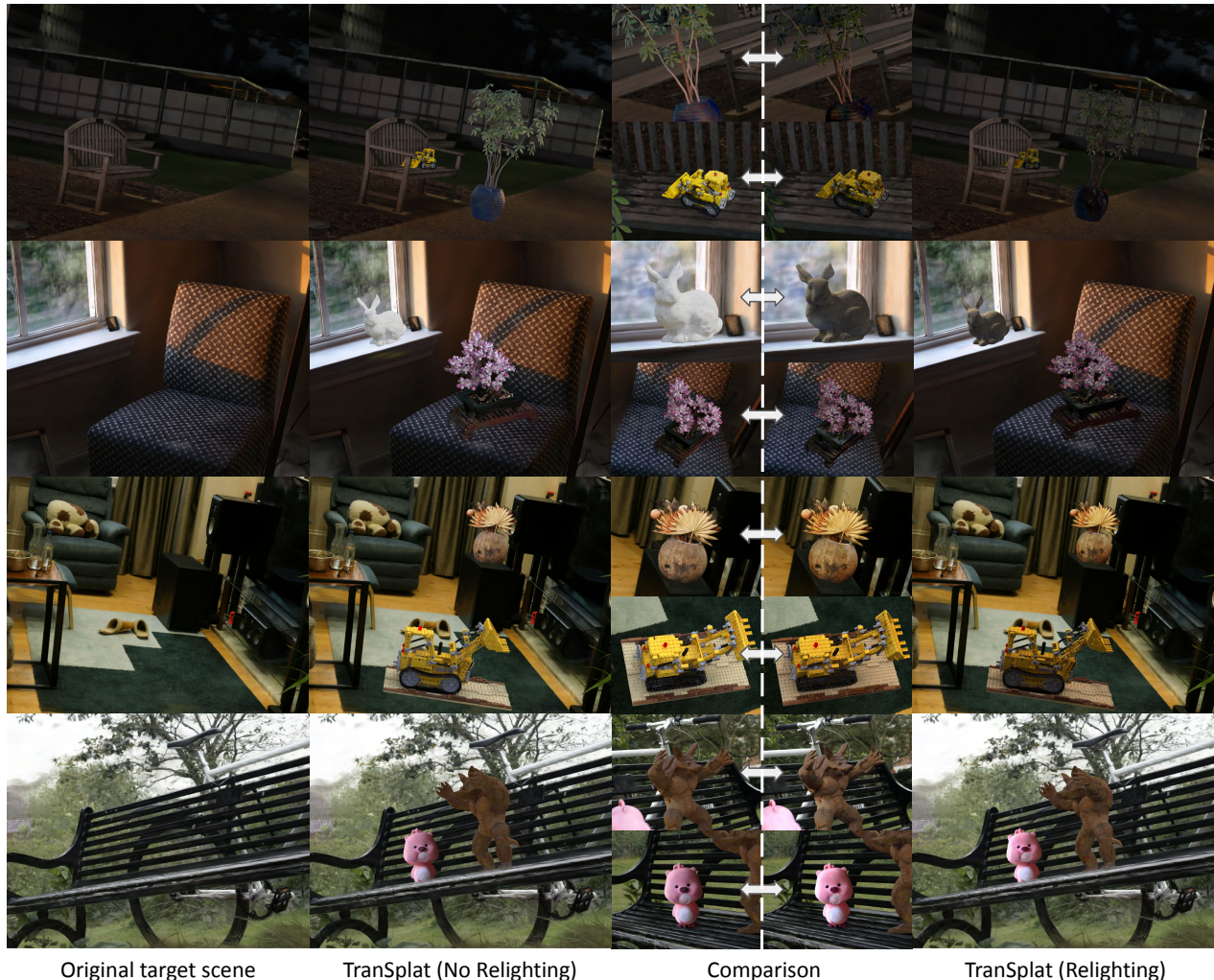


Figure 7. **Sample results demonstrating *TranSplat*'s ability at object transfer and relighting.** We visualize four sets of results taking source objects and transferring them to alternate scenes. Injecting objects into another scene without relighting renders incongruous appearances with unnatural color and illumination, yet with the addition of *TranSplat*'s relighting optimization, renderings appear more natural. We also observe correct correlations, such as when outdoor objects are transferred to an indoor target scene, they exhibit dimmer tones, and vice versa. Details are best observed in Supplementary videos.

consider transmittance (τ) when updating per-Gaussian label weights in Eq. (7), and (2) one that does consider transmittance. We apply the same text prompts and label threshold for both GaussianEditor and *TranSplat*. For SAGA [7], we use the “point prompt”, and evenly distribute five points around each object. Fig. 5 presents results for two scenes (see Supplementary for more examples). *TranSplat* outperforms the baselines at cleanly extracting the objects.

5.2. Relighting Accuracy Results

Next, we compare *TranSplat* against two baseline algorithms (GS-IR [22], TensoIR [17]) on the task of relighting. We use four objects (*Bunny*, *Armadillo*, *Lego*, *Ficus*) and existing HDR maps to relight these objects in Blender. For

a consistent comparison, we use the same source environment (*City*) for all cases. We present numerical results in Table 1, and visual results in Fig. 6. In general, *TranSplat*'s relight renders are closest to ground truth. TensoIR performs well on three of the four objects, but has significant artifacts on *Bunny*. Table 2 presents timing results for these algorithms. *TranSplat* and GS-IR are comparable in training and rendering, while TensoIR is significantly slower.

5.3. Qualitative Object Transfer Results

We selected the room and bike scene from the *MipN-eRF360* [2] dataset and additionally recorded two dark scenes as four target scenes T to showcase *TranSplat*'s capabilities. In each scene, we inserted two objects: one

Table 1. **Quantitative evaluation of relighting methods.** We compare *TranSplat* against GS-IR [22], TensoIR [17] on four TensoIR datasets (lego, armadillo, bunny, ficus) under three environment maps (fireplace, forest, sunset). The best results are highlighted in **bold**. *TranSplat* generally performs the best of the three methods. Refer to Fig. 6 for visual comparisons.

	fireplace			forest			sunset		
	GS-IR	TensoIR	<i>TranSplat</i>	GS-IR	TensoIR	<i>TranSplat</i>	GS-IR	TensoIR	<i>TranSplat</i>
PSNR (dB) ↑									
lego	24.0	29.3	30.7	22.5	27.1	27.2	23.6	27.0	30.6
armadillo	28.0	31.2	32.1	27.3	34.3	34.8	27.7	34.7	34.2
bunny	24.5	17.1	28.7	19.3	16.2	29.6	19.3	15.9	33.0
ficus	29.9	22.0	25.2	27.5	25.7	27.8	28.2	24.3	27.4
SSIM ↑									
lego	0.86	0.92	0.95	0.86	0.93	0.87	0.89	0.93	0.94
armadillo	0.92	0.97	0.94	0.93	0.98	0.97	0.94	0.98	0.97
bunny	0.91	0.89	0.95	0.89	0.89	0.97	0.89	0.89	0.98
ficus	0.97	0.94	0.96	0.96	0.96	0.97	0.97	0.94	0.97
LPIPS ↓									
lego	0.10	0.12	0.05	0.09	0.12	0.10	0.09	0.12	0.05
armadillo	0.07	0.05	0.06	0.07	0.06	0.05	0.06	0.05	0.05
bunny	0.09	0.19	0.07	0.10	0.13	0.07	0.10	0.14	0.07
ficus	0.03	0.07	0.04	0.04	0.05	0.03	0.04	0.06	0.03

Table 2. **Training and rendering times of *TranSplat* and baseline methods.** We report average times using a single A100 40 GB GPU. *TranSplat* is comparable in training and rendering times to GS-IR, and far faster than TensoIR.

	<i>TranSplat</i>	GS-IR [22]	TensoIR [17]
Training time (per scene)	1.5 hr	1 hr	5 hr
Rendering time (per image)	0.3 sec	0.3 sec	10 sec

Blender object with a known source environment (*City*) and another extracted from the source GS scene with our segmentation method. Segmented objects will require additional sampling of the source map at their original position in S . We noticed that for some scenes, the sampled environment can contain missing regions due to unobserved areas in the dataset, such as the sky or ceiling. To address this, we adjusted the GS-rendered background to better match the colors of the walls or the sky.

We compare objects inserted using *TranSplat* before and after relighting in Fig. 7. Directly inserting objects into T often results in unrealistic lighting appearances. For example, the ficus from *TensoIR* [17] appears overly bright in a nighttime scene, while the Armadillo looks too dark when placed on an outdoor bench. Beyond overall brightness differences, realistic shading effects also emerged. For instance, in the second row, the bunny appears brighter on the side facing the window, and the vase in the third row from the original *MipNeRF* garden scene takes on a darker tone at the base when placed into the room scene.

6. Discussion and Limitations

Results demonstrate that *TranSplat*'s two main contributions: improved 3D object extraction from GS models and cross-environment relighting are both competitive or superior to state-of-the-art baselines. Relighting results in Ta-

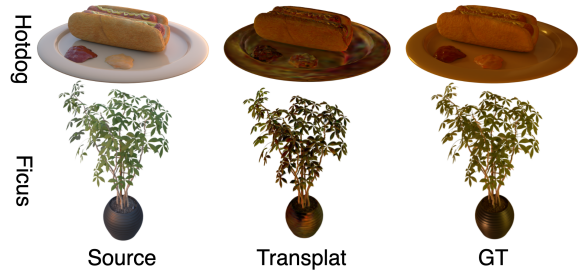


Figure 8. **Failure cases for object relighting due to non-Lambertian effects.** We present relighting results using *TranSplat* on two objects from the TensoIR [17], moving from the *City* source environment to *Fireplace* target. For non-specular regions such as the hotdog and branches of the Ficus, *TranSplat* deliver reasonable, though still flawed color tones. However, *TranSplat* fails to recover accurate colors for specular regions such as the plate and sauces near the hotdog, and the ficus pot.

ble 1 and Fig. 6 show that *TranSplat* is consistently better than two excellent neural relighting baselines on near-Lambertian surfaces. TensoIR [17] and GS-IR [22] have more extreme failure cases, likely due to failure in estimating underlying scene/material properties. In contrast, *TranSplat* is more stable, and works well for both indoor and outdoor cross-scene tasks (see Fig. 7).

There are several limitations of this study. First, *TranSplat*'s model of light rendering is simplistic. It assumes that the object has a radially symmetric BRDF, and does not explicitly take into account non-global lighting effects, such as inter-object reflections. This is in contrast to algorithms based on physically-based rendering models that can capture these complexities. Fig. 8 presents two cases where *TranSplat*'s relighting results are not satisfactory due to these assumptions not holding. Second, we observe that the off-the-shelf LDR-to-HDR model [23] we use to generate environment maps (see Sec. 4.3) struggles at maintaining a consistent scale of values between the source and target environment maps. Third, *TranSplat* is not yet scalable for large dataset synthesis due to the need for human user input in object insertion. An interesting future line of work is to develop methods to automatically suggest the position and scale of an object in a target scene.

Acknowledgements

Supported by the Intelligence Advanced Research Projects Activity (IARPA) via Department of Interior/ Interior Business Center (DOI/IBC) contract number 140D0423C0076. The U.S. Government is authorized to reproduce and distribute reprints for Governmental purposes notwithstanding any copyright annotation thereon. Disclaimer: The views

and conclusions contained herein are those of the authors and should not be interpreted as necessarily representing the official policies or endorsements, either expressed or implied, of IARPA, DOI/IBC, or the U.S. Government.

References

- [1] Jonathan T Barron, Ben Mildenhall, Matthew Tancik, Peter Hedman, Ricardo Martin-Brualla, and Pratul P Srinivasan. Mip-nerf: A multiscale representation for anti-aliasing neural radiance fields. In *Proceedings of the IEEE/CVF International Conference on Computer Vision*, pages 5855–5864, 2021. 2
- [2] Jonathan T. Barron, Ben Mildenhall, Dor Verbin, Pratul P. Srinivasan, and Peter Hedman. Mip-nerf 360: Unbounded anti-aliased neural radiance fields. 2022. 2, 5, 7
- [3] Ronen Basri and David W Jacobs. Lambertian reflectance and linear subspaces. *IEEE transactions on pattern analysis and machine intelligence*, 25(2):218–233, 2003. 3
- [4] Jeremy Birn. *Digital lighting & rendering*. Pearson Education, 2014. 2
- [5] Samuel Boivin and André Gagalowicz. Image-based rendering of diffuse, specular and glossy surfaces from a single image. In *Proceedings of the 28th annual conference on Computer graphics and interactive techniques*, pages 107–116, 2001. 2
- [6] Mark Boss, Raphael Braun, Varun Jampani, Jonathan T Barron, Ce Liu, and Hendrik Lensch. Nerf: Neural reflectance decomposition from image collections. In *Proceedings of the IEEE/CVF International Conference on Computer Vision*, pages 12684–12694, 2021. 2
- [7] Jiazhong Cen, Jiemin Fang, Chen Yang, Lingxi Xie, Xiaopeng Zhang, Wei Shen, and Qi Tian. Segment any 3d gaussians. *arXiv preprint arXiv:2312.00860*, 2023. 5, 6, 7
- [8] Minghao Chen, Iro Laina, and Andrea Vedaldi. Dge: Direct gaussian 3d editing by consistent multi-view editing. *arXiv preprint arXiv:2404.18929*, 2024. 2, 3
- [9] Yiwen Chen, Zilong Chen, Chi Zhang, Feng Wang, Xiaofeng Yang, Yikai Wang, Zhongang Cai, Lei Yang, Huaping Liu, and Guosheng Lin. Gaussianeditor: Swift and controllable 3d editing with gaussian splatting. In *Proceedings of the IEEE/CVF conference on computer vision and pattern recognition*, pages 21476–21485, 2024. 2, 3, 4, 5, 6
- [10] Pinxuan Dai, Jiamin Xu, Wenxiang Xie, Xinguo Liu, Huamin Wang, and Weiwei Xu. High-quality surface reconstruction using gaussian surfels. In *ACM SIGGRAPH 2024 Conference Papers*. Association for Computing Machinery, 2024. 2, 3, 4
- [11] Paul Debevec, Chris Tchou, Andrew Gardner, Tim Hawkins, Charis Poullis, Jessi Stumpfel, Andrew Jones, Nathaniel Yun, Per Einarsson, Therese Lundgren, et al. Estimating surface reflectance properties of a complex scene under captured natural illumination. *Conditionally Accepted to ACM Transactions on Graphics*, 19:2, 2004. 2
- [12] Frédéric Durand, Nicolas Holzschuch, Cyril Soler, Eric Chan, and François X Sillion. A frequency analysis of light transport. *ACM Transactions on Graphics (TOG)*, 24(3):1115–1126, 2005. 2
- [13] Martin A Fischler and Robert C Bolles. Random sample consensus: a paradigm for model fitting with applications to image analysis and automated cartography. *Communications of the ACM*, 24(6):381–395, 1981. 5, 11
- [14] Jian Gao, Chun Gu, Youtian Lin, Hao Zhu, Xun Cao, Li Zhang, and Yao Yao. Relightable 3d gaussian: Real-time point cloud relighting with brdf decomposition and ray tracing. *arXiv:2311.16043*, 2023. 2, 3
- [15] Daniel Girardeau-Montaut et al. Cloudcompare. *France: EDF R&D Telecom ParisTech*, 11(5):2016, 2016. 5
- [16] Yingwenqi Jiang, Jiadong Tu, Yuan Liu, Xifeng Gao, Xiaoxiao Long, Wenping Wang, and Yuexin Ma. Gaussian-shader: 3d gaussian splatting with shading functions for reflective surfaces. In *Proceedings of the IEEE/CVF Conference on Computer Vision and Pattern Recognition*, pages 5322–5332, 2024. 2, 3
- [17] Haian Jin, Isabella Liu, Peijia Xu, Xiaoshuai Zhang, Songfang Han, Sai Bi, Xiaowei Zhou, Zexiang Xu, and Hao Su. Tensor: Tensorial inverse rendering. In *Proceedings of the IEEE/CVF Conference on Computer Vision and Pattern Recognition (CVPR)*, 2023. 2, 3, 5, 6, 7, 8
- [18] James T. Kajiya. The rendering equation. page 4, 1986. 3
- [19] Bernhard Kerbl, Georgios Kopanas, Thomas Leimkühler, and George Drettakis. 3d gaussian splatting for real-time radiance field rendering. *ACM Transactions on Graphics*, 42(4), 2023. 1, 2, 3
- [20] Alexander Kirillov, Eric Mintun, Nikhila Ravi, Hanzi Mao, Chloe Rolland, Laura Gustafson, Tete Xiao, Spencer Whitehead, Alexander C Berg, Wan-Yen Lo, et al. Segment anything. In *Proceedings of the IEEE/CVF international conference on computer vision*, pages 4015–4026, 2023. 3, 4
- [21] Zhengqi Li, Wenqi Xian, Abe Davis, and Noah Snavely. Crowdsampling the plenoptic function. In *Computer Vision—ECCV 2020: 16th European Conference, Glasgow, UK, August 23–28, 2020, Proceedings, Part I 16*, pages 178–196. Springer, 2020. 2
- [22] Zhihao Liang, Qi Zhang, Ying Feng, Ying Shan, and Kui Jia. Gs-ir: 3d gaussian splatting for inverse rendering. *arXiv preprint arXiv:2311.16473*, 2023. 2, 3, 6, 7, 8
- [23] Yu-Lun Liu, Wei-Sheng Lai, Yu-Sheng Chen, Yi-Lung Kao, Ming-Hsuan Yang, Yung-Yu Chuang, and Jia-Bin Huang. Single-image hdr reconstruction by learning to reverse the camera pipeline. In *Proceedings of the IEEE/CVF conference on computer vision and pattern recognition*, pages 1651–1660, 2020. 5, 8
- [24] Dhruv Mahajan, Ravi Ramamoorthi, and Brian Curless. A theory of spherical harmonic identities for brdf/lighting transfer and image consistency. In *Computer Vision – ECCV 2006*, pages 41–55. Springer, Heidelberg, 2006. 2, 3, 5
- [25] Stephen Robert Marschner. *Inverse rendering for computer graphics*. Cornell University, 1998. 2
- [26] Ricardo Martin-Brualla, Noha Radwan, Mehdi SM Sajjadi, Jonathan T Barron, Alexey Dosovitskiy, and Daniel Duckworth. Nerf in the wild: Neural radiance fields for unconstrained photo collections. In *Proceedings of the IEEE/CVF*

- conference on computer vision and pattern recognition, pages 7210–7219, 2021. 2
- [27] Aryan Mikaeili, Or Perel, Mehdi Safaei, Daniel Cohen-Or, and Ali Mahdavi-Amiri. Sked: Sketch-guided text-based 3d editing. In *Proceedings of the IEEE/CVF International Conference on Computer Vision*, pages 14607–14619, 2023. 3
- [28] Ben Mildenhall, Pratul P Srinivasan, Matthew Tancik, Jonathan T Barron, Ravi Ramamoorthi, and Ren Ng. Nerf: Representing scenes as neural radiance fields for view synthesis. *Communications of the ACM*, 65(1):99–106, 2021. 2
- [29] Ravi Ramamoorthi and Pat Hanrahan. A signal-processing framework for inverse rendering. In *Proceedings of the 28th annual conference on Computer graphics and interactive techniques*, pages 117–128, 2001. 2, 3
- [30] Shunsuke Saito, Gabriel Schwartz, Tomas Simon, Junxuan Li, and Giljoo Nam. Relightable gaussian codec avatars. In *Proceedings of the IEEE/CVF conference on computer vision and pattern recognition*, pages 130–141, 2024. 3
- [31] Shen Sang and Manmohan Chandraker. Single-shot neural relighting and svbrdf estimation. In *Computer Vision—ECCV 2020: 16th European Conference, Glasgow, UK, August 23–28, 2020, Proceedings, Part XIX 16*, pages 85–101. Springer, 2020. 2
- [32] Hyeonseop Song, Seokhun Choi, Hoseok Do, Chul Lee, and Taehyeong Kim. Blending-nerf: Text-driven localized editing in neural radiance fields. In *Proceedings of the IEEE/CVF International Conference on Computer Vision*, pages 14383–14393, 2023. 3
- [33] Pratul P Srinivasan, Boyang Deng, Xiuming Zhang, Matthew Tancik, Ben Mildenhall, and Jonathan T Barron. Nerv: Neural reflectance and visibility fields for relighting and view synthesis. In *Proceedings of the IEEE/CVF conference on computer vision and pattern recognition*, pages 7495–7504, 2021. 3
- [34] Can Wang, Menglei Chai, Mingming He, Dongdong Chen, and Jing Liao. Clip-nerf: Text-and-image driven manipulation of neural radiance fields. In *Proceedings of the IEEE/CVF Conference on Computer Vision and Pattern Recognition*, pages 3835–3844, 2022. 3
- [35] Yao Yao, Jingyang Zhang, Jingbo Liu, Yihang Qu, Tian Fang, David McKinnon, Yanghai Tsin, and Long Quan. Neilf: Neural incident light field for physically-based material estimation. In *European conference on computer vision*, pages 700–716. Springer, 2022. 3
- [36] Ye Yu and William AP Smith. Inverserendernet: Learning single image inverse rendering. In *Proceedings of the IEEE/CVF Conference on Computer Vision and Pattern Recognition*, pages 3155–3164, 2019. 2
- [37] Yu-Jie Yuan, Yang-Tian Sun, Yu-Kun Lai, Yuewen Ma, Rongfei Jia, and Lin Gao. Nerf-editing: geometry editing of neural radiance fields. In *Proceedings of the IEEE/CVF Conference on Computer Vision and Pattern Recognition*, pages 18353–18364, 2022. 3
- [38] Jingyang Zhang, Yao Yao, Shiwei Li, Jingbo Liu, Tian Fang, David McKinnon, Yanghai Tsin, and Long Quan. Neilf++: Inter-reflectable light fields for geometry and material estimation. In *Proceedings of the IEEE/CVF International Conference on Computer Vision*, pages 3601–3610, 2023. 3
- [39] Xiuming Zhang, Pratul P Srinivasan, Boyang Deng, Paul Debevec, William T Freeman, and Jonathan T Barron. Nerfactor: Neural factorization of shape and reflectance under an unknown illumination. *ACM Transactions on Graphics (ToG)*, 40(6):1–18, 2021. 3
- [40] Jingyu Zhuang, Di Kang, Yan-Pei Cao, Guanbin Li, Liang Lin, and Ying Shan. Tip-editor: An accurate 3d editor following both text-prompts and image-prompts. *arXiv preprint arXiv:2401.14828*, 2024. 3

Supplementary Material for TranSplat

A. Relighting Demonstration Videos

To better illustrate the relighting effect of *TranSplat*, we generated videos of the results in the paper using two common visualization methods: sliders and fading. Please refer to the videos within the supplementary material package.

B. Additional Segmentation Results

We present additional semantic segmentation results in Fig. 9. Please also refer to the provided video in the supplementary zip file showing the rotating views of the extracted bicycle and the extracted background (object removal). For background extraction, we simply selected Gaussians with label scores lower than a threshold. In the video, *TranSplat* achieves the cleanest Gaussian removal of the background in the distance, while neither baseline method is able to completely remove the bike even by adjusting the weight thresholds.

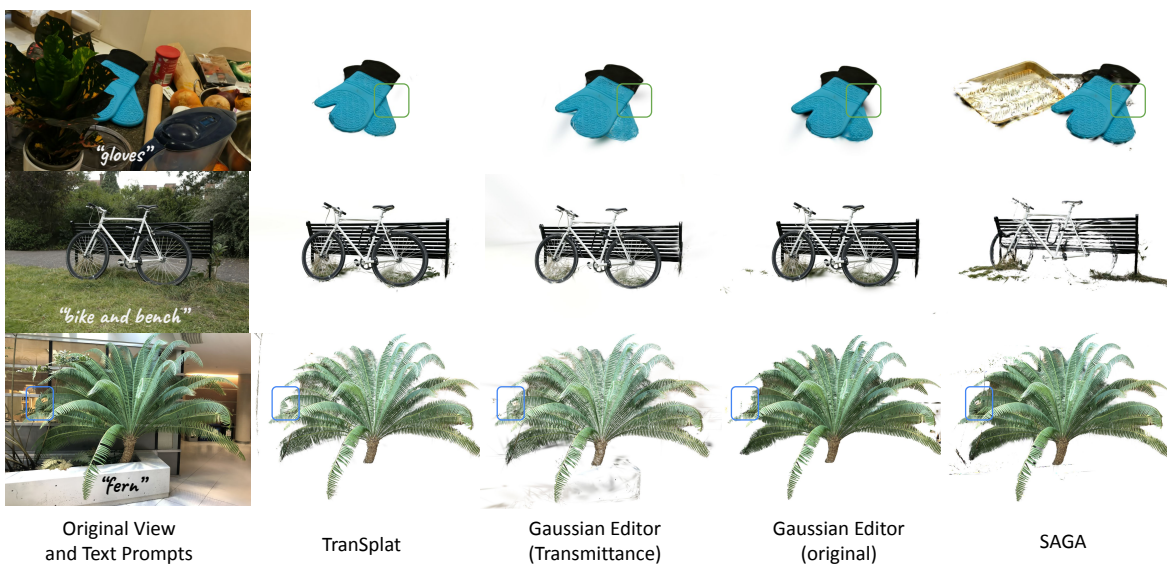


Figure 9. **Additional object extraction/segmentation results.** This figure presents additional examples to Fig. 5 in the main paper comparing *TranSplat* to two segmentation baselines.

C. Object Insertion Details and Example

Once an object is extracted from the source scene, we ask a user to roughly place the object (via GUI interface) at the intended 3D location in T , and specify a rescale factor α to adjust the object’s size as needed. We apply α to the positions ($x' = \alpha x, y' = \alpha y, z' = \alpha z$) and standard deviations ($s' = s + \ln(\alpha)$) of every Gaussian in the object.

Next, we automatically refine the orientation and position of the object in T by assuming that the object was located on a flat surface (e.g., the ground or a table) in S , and is intended to sit on the nearest flat surface in T . We first estimate local planes around the object’s neighborhoods in S and T using RANSAC [13] on Gaussians. Using the normal vectors of these planes, we generate a rotation matrix which we apply to the position and quaternion attributes of each Gaussian in the object. Finally, to refine the object’s position to sit directly on the flat surface, we translate the object along the vector \mathbf{n}_T until any Gaussian on the object intersects any Gaussian on the surface plane. Fig. 10 shows an example of inserting an object into a scene, after adjusting for scale, rotation, and position with our process.

D. Weighted Sampling for Environment Map to SH Conversion

We compared two methods for sampling colors from the environment map: weighted and unweighted. For weighted sampling, we multiply the equations that link SH base functions to colors by $\sqrt{\sin \theta}$, yielding a weighted least-squares formulation



Figure 10. **Example of automatic object rotation and translation adjustment of a bike inserted into a table.** Object insertion consists of four steps: rough positioning and scaling (user-based), followed by rotation and translation to the nearest surface (automated).

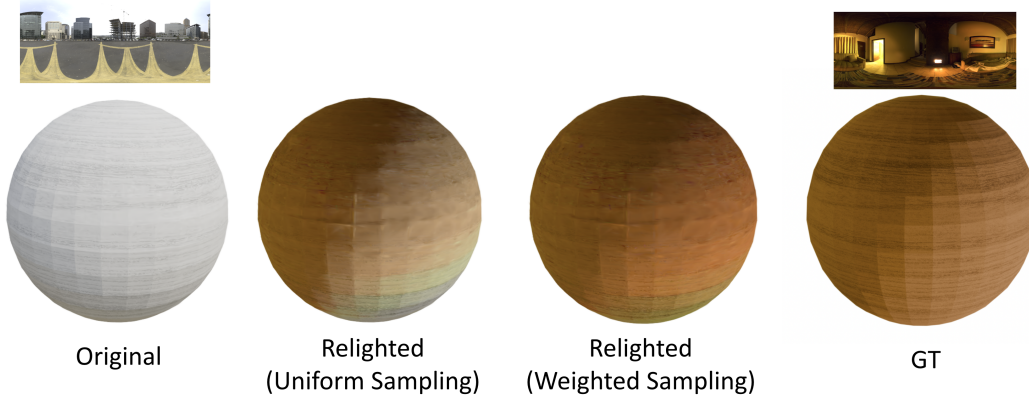


Figure 11. **Experiments on the choice of color sampling method.** The original sphere was under the city environment condition, and we use *Transplat* to relight it to match the appearance under the fireplace environment. However, uniform sampling leads to inaccuracies when converting the environment map to SH, causing larger color deviations and the appearance of unintended green hues.

for solving SH coefficients of the environment map. Fig. 11 demonstrates the advantage of weighted sampling on a simple sphere, rendered in two environments. We used the same number of environment map samples (5000) for both unweighted and weighted cases. Unweighted sampling results in a green hue at the bottom of the sphere, while weighted achieves a result close to ground truth.